Title: Viral-mediated Oct4 overexpression and inhibition of Notch signaling synergistically induce neurogenic competence in mammalian Müller glia.

Authors: Nguyet Le [1], Sherine Awad[6-8], Isabella Palazzo[1], Thanh Hoang[6-8], Seth Blackshaw[1-5]*

1 Department of Neuroscience,
2 Department of Ophthalmology,
3 Department of Neurology,
4 Institute for Cell Engineering,
5 Kavli Neuroscience Discovery Institute,
Johns Hopkins University School of Medicine, Baltimore, MD 21205
6 Department of Ophthalmology and Visual Sciences, University of Michigan School of Medicine, Ann Arbor, MI 48105
7 Department of Cell and Developmental Biology, University of Michigan School of Medicine, Ann Arbor, MI 48105
8 Michigan Neuroscience Institute, University of Michigan School of Medicine, Ann Arbor, MI 48105
*To whom correspondence should be addressed.

Abstract: Retinal Müller glia in cold-blooded vertebrates can reprogram into neurogenic progenitors to replace neurons lost to injury, but mammals lack this ability. While recent studies have shown that transgenic overexpression of neurogenic bHLH factors and glial-specific disruption of NFI family transcription factors and Notch signaling induce neurogenic competence in mammalian Müller glia, induction of neurogenesis in wildtype glia has thus far proven elusive. Here we report that viral-mediated overexpression of the pluripotency factor *Oct4* (*Pou5f1*) induces transdifferentiation of wildtype mouse Müller glia into bipolar neurons, and synergistically stimulates glial-derived neurogenesis in parallel with Notch loss of function. Single cell multiomic analysis shows that *Oct4* overexpression leads to widespread changes in gene expression and chromatin accessibility, inducing activity of both the neurogenic transcription factor Rfx4 and the Yamanaka factors Sox2 and Klf4. This study demonstrates that viral-mediated overexpression of Oct4 induces neurogenic competence in wildtype retinal Muller glia, identifying mechanisms that could be used in cell-based therapies for treating retinal dystrophies.

Introduction: The homeodomain factor Oct4 (Pou5f1) is a central component of transcriptional regulatory networks that maintain pluripotency in embryonic stem (ES) cells. Along with Sox2, Klf4, and Myc, Oct4 is one of the Yamanaka factors sufficient to induce the formation of induced pluripotent stem cells (iPSCs) from virtually all somatic cell types (Takahashi and Yamanaka, 2006). In contrast to these other factors, *Oct4* is selectively expressed in ES cells and essentially absent from somatic cells, including adult stem cells from every tissue examined. The two clear exceptions are found in gonadal stem cells (Takashima et al., 2013; Uhlen et al., 2010) and during neural crest formation, where *Oct4* expression is essential for the ability of these cells to generate diverse cell types (Morrison and Brickman, 2006; Zalc et al., 2021). This has raised the question of whether *Oct4* overexpression *in vivo*,

alone or in combination with other pluripotency factors, may confer some level of multipotency on somatic cells in the central nervous system.

Sustained overexpression of the Yamanaka factors *Oct4*, *Sox2*, *Klf4,* and *Myc* induces teratoma formation in many tissues (Abad et al., 2013; Ohnishi et al., 2014). Transient or low-level Yamanaka factor overexpression, in contrast, has been reported to induce cellular rejuvenation in both neurons and other cell types, although this occurs without clear induction of proliferation or conferring multipotency (Ocampo et al., 2016; C. Wang et al., 2021). However, several studies have directly investigated whether viral-mediated overexpression in CNS neural stem or glial cells of Oct4 alone, or in combination with subsets of other pluripotency factors, can induce multipotency and neurogenesis. Results from these studies are mixed, with *Oct4* overexpression in neural stem cells reported to either not induce neurogenesis (Asadi et al., 2015; Dehghan et al., 2015; Sim et al., 2011), to promote formation of oligodendrocyte progenitors (OPCs) (Yu et al., 2021), or to promote remyelination in committed OPCs (Dehghan et al., 2016). Two studies reported that viral-mediated *Oct4* overexpression, either alone (Niu et al., 2013) or in combination with other Yamanaka factors (Gao et al., 2016), could directly convert reactive astrocytes into neurons. However, these studies used the GFAP minipromoter to drive gene expression, which has been reported to show insert-dependent ectopic insert-dependent silencing in glia and activation in neurons (L.-L. Wang et al., 2021). This limitation makes these findings difficult to interpret, as additional methods of validating cell lineage were not used.

Two previous studies have reported injury-dependent induction of *Oct4* in retinal Müller glial cells in zebrafish and mice. In zebrafish, where injury induces Müller glia to undergo conversion to neurogenic progenitors (Wan and Goldman, 2016), it was reported that *Oct4* is essential for glial reprogramming to occur (Sharma et al., 2019). In mice, where neurogenic competence is rapidly and actively suppressed following injury, it was reported that *Oct4* expression is transiently induced, but fully repressed within 24 hours following injury (Reyes-Aguirre and Lamas, 2016). This raises the possibility that *Oct4* expression may be sufficient to confer neurogenic competence on retinal Müller glial cells. In this study, we assessed whether AAV-mediated overexpression of Oct4 could induce reprogramming of adult mouse Müller glia. While we did not detect any expression of *Oct4* in either zebrafish or mouse Müller glia following injury, we use both genetic cell lineage and single-cell omics analyses to unambiguously demonstrate that viral-mediated overexpression of *Oct4* selectively induces the formation of bipolar neurons from wildtype mouse Müller glia without inducing substantial levels of proliferation. We further show that *Oct4* overexpression synergistically enhances existing levels of Müller glia-derived neurogenesis in the absence of Notch signaling. Single-cell multiomic analysis demonstrates that Oct4 cooperates with Sox2 and Klf4, which are constitutively expressed in Müller glia, to broadly alter the gene regulatory landscape and induce expression of genes such as the neurogenic transcription factor *Rfx4*. This demonstrates that substantial levels of *in situ* glia-to-neuron reprogramming in mammalian retina can be induced by viral overexpression of a key Yamanaka factor.

Results:

Oct4 and Nanog are not detectably expressed in Müller glia or Müller glia-derived progenitor cells in either zebrafish or mice

To examine the expression of *Oct4* and other pluripotency-associated genes in wildtype and neurogenic Müller glia, we analyzed bulk and single-cell RNA-Seq data previously generated by our group from zebrafish and mice (Hoang et al., 2020). Consistent with previous findings (Nelson et al., 2011; Surzenko et al., 2013), in mice we detected expression of *Sox2* and *Klf4* in resting and both NMDA-treated and light-damaged Müller glia, along with injury-induced expression of *Myc*. Likewise, in zebrafish we observe expression of *sox2* and *myca/b* (but not *klf4*) in both resting and injured Müller glia (Fig. S1a,b). However, we did not detect expression of either *Oct4* or its direct target *Nanog* in either species in any treatment condition (Loh et al., 2006). Bulk RNA-Seq data obtained from purified Müller glia detected very low levels of *Oct4* (*pou5f3*), but not Nanog, expression in some injured zebrafish Muller glia, but neither *Oct4* nor *Nanog* was detected in either resting or injured mouse Müller glia (Fig. S1a,b). Similarly, we did not observe any induction of *Oct4* in snRNA-Seq data from mouse Müller glia made neurogenic by selective loss of function of *Rbpj* alone or in combination with *Nfia/b/x* (Le et al., 2024) (Fig. S1c). These results indicate that neither NMDA excitotoxicity, light damage, or induction of neurogenic competence by loss of function of *Nfia/b/x* and/or *Rbpj* induces detectable levels of *Oct4* or *Nanog* in neurogenic mammalian Müller glia.

AAV-mediated overexpression of *Oct4* induces conversion of wildtype mouse Müller glia to bipolar-like cells

To determine whether *Oct4* overexpression could reprogram mammalian Müller glia into a neurogenic state, we administered intraperitoneal tamoxifen injections into P21 *GlastCreER;Sun1-GFP* mice, irreversibly labeling Müller glia with Sun1-GFP (de Melo et al., 2012; Hoang et al., 2020) (Fig. S2a, Fig. 1a). One week following the final tamoxifen dose, we performed intravitreal injections of either Gfap-Oct4-mCherry or Gfap-mCherr*y* control 7m8 AAV. While expression of neurogenic bHLH factors driven by the Gfap promoter were rapidly silenced in Müller glia and activated in amacrine and retinal ganglion cells, Gfap-Oct4-mCherry remained selectively expressed in Müller glia but did not induce detectable levels of Müller glia-derived neurogenesis in the uninjured retina (Le et al., 2022). To assess whether excitotoxic injury could promote neurogenic competence, we injected N-methyl-d-aspartate (NMDA) (Hoang et al., 2020) one week post-viral injection. We then administered EdU following NMDA injection for one week to label proliferating cells. Retinas were harvested and analyzed at 1, 2, and 5 weeks post-injury (Fig. S2b, Fig. 1b).

Immunostaining analysis revealed enriched mCherry expression in Müller glia in both control mCherry and Oct4-mCherry infected retinas at all timepoints (Fig. 1C, Fig. S2). In addition, Oct4 expression was detected in GFP-positive Müller glia in Oct4-mCherry infected retinas but not in mCherry control retina (Fig. S2i-j, S3i-j, S4a). We also observed selective expression of the neurogenic bHLH factor Ascl1 in Oct4-mCherry infected Müller glia at 1 week post-injury, with the number of Ascl-positive cells declining somewhat by 2 weeks post-injury (Fig. S2e,f). While Sun1-GFP-positive cells infected with Oct4-mCherry mostly express the Müller glial marker Sox2 (Fig. S2a,b), from 2 weeks post-injury onwards a subset of GFP-positive cells did not show detectable Sox2 expression (Fig. S2b, yellow arrows).

At 1 week post-injury, we did not observe any significant Müller glia-derived neurogenesis. By 2 weeks post-injury, 1.1% of GFP-positive cells co-localized with the bipolar cell marker Otx2 in Oct4-mCherry infected retinas (Fig. S2k,l,n), and this increased to 5.1% of GFP-positive cells at 5 weeks post-injury (Fig. 1c,d). We observed that Müller glia-derived Otx2+ neurons show little or no mCherry reporter expression, due to reduced activity of the Gfap minipromoter in neurons. Immunostaining with additional cell-specific markers revealed that a subset of these GFP-positive cells expressed the cone bipolar markers Scgn and Cabp5 (Fig. S3d,e), but not the rod and cone ON bipolar cell marker Isl1 or the rod marker Nrl (Fig. S3f,g). Furthermore, we did not observe expression of the amacrine cell marker HuC/D in GFP-positive cells (Fig. 1c,d), which is observed in neurons generated from neurogenic mouse Müller glia deficient in either *Rbpj* or *Nfia/b/x* (Hoang et al., 2020; Le et al., 2024).

To test whether Oct4 overexpression could induce proliferation in wildtype Müller glia, we administered 5-ethynyl-2'-deoxyuridine (EdU) through daily intraperitoneal injections and drinking water following NMDA injury. At 2 weeks post-injury, we observed a very limited number of GFP-positive cells incorporating EdU in retinas infected with both mCherry control and Oct4-mCherry, with EdU incorporation in the second post-injury week modestly but significantly increased by *Oct4* overexpression (Fig. S2f,n). However, no EdU/GFP-positive cells were detected at either 1 week (Fig. S2e,n) or 5 weeks post-injury (Fig. S4h). These findings indicate that Oct4 overexpression induces a very low level of proliferation in wildtype Müller glia in the second week following NMDA injury. However, the absence of EdU/Otx2/GFP-positive cells at both 2 and 5 weeks post-injury suggests that bipolar cell generation at this stage was, at least in part, driven by direct transdifferentiation.

***Oct4* overexpression synergistically enhances glial-derived neurogenesis induced by genetic disruption of Notch signaling**

In our previous study, we demonstrated that disrupting Notch signaling in adult mouse Müller glia–either by selective deletion of the transcriptional mediator *Rbpj* or by combined disruption of *Notch1* and *Notch2* receptors–induces transdifferentiation into bipolar and amacrine-like cells (Le et al. 2024). To further determine the effects of *Oct4* overexpression in the absence of Notch signaling, we used *GlastCreER;Rbpj*$^{lox/lox}$*;Sun1-GFP* mice to genetically label Müller glia while disrupting *Rbpj* function (Fig. 2a, S4a). We then performed intravitreal injection of either control or *Oct4* overexpression constructs, followed by NMDA and EdU injection as performed for *GlastCreER;Sun1-GFP* mice. Retinas were collected at 1 , 2 and 5 weeks following NMDA treatment (Fig. 2b, S4b). Immunostaining confirmed expression of Oct4 protein in GFP-positive Müller glia of Oct4-mCherry infected retinas, but not in mCherry-infected controls (Fig. S3j, S4i,j). We observed that many GFP-positive cells in Oct4-mCherry-infected retinas did not express the Müller glial markers Sox2 (Fig.S4c,d) and Sox9 (Fig. S3j, yellow arrows), suggesting that they have lost their glial identity.

Five weeks following NMDA injury, we observed 4.5% of GFP-positive cells in retinas of mCherry-infected controls expressed the bipolar cell marker Otx2, while 0.7% expressed the amacrine cell marker HuC/D (Fig. 2c,d). These levels of neurogenesis are consistent with previous findings in uninfected *Rbpj*-deficient Müller glia (Le et al., 2024). In contrast, we

observe 24.3% of GFP-positive cells expressing Otx2 in Oct4-mCherry-infected retinas, representing a significant ($p < 0.0001$) increase relative to control. However, we did not observe a significant change in the relative fraction of GFP/HuC/D-double-positive cells. In contrast to wildtype retinas, no EdU incorporation was detected in *Oct4*-expressing, *Rbpj*-deficient Müller glia at either 1 or 2 weeks following infection (Fig. S4e,f), indicating that the observed neurogenesis is due largely to direct transdifferentiation of Müller glia into retinal neuron-like cells, rather than through dedifferentiation to a proliferative neuronal progenitor-like state.

Next, we tested whether Oct4 overexpression could further enhance neurogenesis in other cell-specific mutants that induce neurogenic competence in adult Müller glia. We have previously observed Müller glia-specific *Notch1/2* double mutants phenocopy neurogenesis seen in Rbpj mutants (Le et al., 2024). To do this, we used *GlastCreER;Notch1$^{lox/lox}$;Notch2$^{lox/lox}$;Sun1-GFP* mice (Fig. S5a), and analyzed the effect of *Oct4* overexpression using the same protocol previously described for wildtype and *Rbpj* mutants (Fig. S5b). We observed 15.8% of GFP+ Müller glia colocalized with Otx2 in Oct4-mCherry-infected retinas compared to 6.6% GFP/Otx2+ cells in samples infected with control mCherry vector (Fig. S5c). Infection with Oct4-mCherry vector induced both Oct4 (Fig. S5e) and Ascl1 (Fig. S5d) expression in *Notch1/2*-deficient Müller glia.

Finally, we also tested whether *Oct4* overexpression could enhance Müller glia-derived neurogenesis induced by loss of function of the transcription factors *Nfia*, *Nfib*, and *Nfix* (Hoang et al., 2020). *GlastCreER;Nfia$^{lox/lox}$;Nfib$^{lox/lox}$;Nfix$^{lox/lox}$;Sun1-GFP* mice (Fig. S6a) were infected with both mCherry and Oct4-mCherry vectors as previously described, and harvested at 5 weeks following NMDA infection (Fig. S6b). However, we observed only very limited coexpression of mCherry and GFP following infection with either construct (Fig. S6c), indicating that NFI factors may be required for appropriate glial-specific expression of the GFAP minipromoter construct, as suggested by previous studies in astrocytes (Cebolla and Vallejo, 2006).

Oct4 overexpression promotes expression of reactive glial markers and neurogenic bHLH factors

To gain insight into the mechanism by which Oct4 stimulates neurogenesis in *Rbpj*-deficient Müller glia, we conducted single-cell (sc)RNA-Seq analysis of GFP-positive cells FACS-isolated from retinas of *GlastCreER;Rbpj$^{lox/lox}$;Sun1-GFP* mice infected with either GFAP-mCherry control or GFAP-Oct4-mCherry virus. Retinas were tamoxifen- and NMDA-treated as described in Figure 2, and GFP-positive cells isolated at 8 weeks following NMDA treatment (Fig. 3a). We profiled 12,143 GFP+ cells from control-infected and 14,612 GFP+ cells from Oct4-mCherry-infected retinas (Fig. 3b). In both samples, we observe a clear differentiation trajectory connecting Müller glia, neurogenic Müller glia-derived progenitor cells (MGPCs), and differentiating amacrine and bipolar cells (Fig. 3b). Oct4-infected retinas consistently show substantially higher fractions of bipolar cells (20.5 % vs. 2.7 %), and a smaller fraction of Müller glia (71.4 % vs. 88.2 %), consistent with immunohistochemical data (Fig. 3c).

Selective molecular markers could readily distinguish Müller glia (*Glul*, *Apoe*, *Vim*, *Clu*, *Rlbp1*) from neurogenic MGPCs (*Neurog2*, *Ascl1*, *Sox4*, *Hes6*, *Dll1*), and clearly identified differentiating bipolar (*Otx2*, *Pcp2*, *Pcp4*, *Car10*, *Gabrb3*) and amacrine-like cells (*Nrxn1*, *Tfap2b*, *Nrg1*, *Snap25*) (Fig. 3d-f, Fig.S7, Table ST1). In both MGs and MGPCs, we observed substantial differences in gene expression between samples infected with control and Oct4-mCherry samples. Oct4-infected Müller glia selectively downregulated genes specific to resting Müller glia (*Car2*, *Dkk3*, *Glul*, *Col23a1, Abca8a*), and upregulated genes enriched in reactive glia (*Gfap*, *Socs3*, *Nupr1*, *Mt1/2/3*, *Fos*, *Jun*, *Klf6*) (Fig. 3e,f, Table ST1). In MGPCs, Oct4 also downregulated both transcription factors (*Lhx2*, *Hopx*) and other genes (*Apoe*, *Dio1*, *Il33*, *Espn*) that are enriched in resting Müller glia, and upregulated many genes selectively expressed in activated glia (*Mt1/2/3*, *Fos*, *Jun*, *Nupr1, Socs3*). In addition, Oct4-infected MGPCs expressed consistently higher levels of neurogenic bHLH factors (*Ascl1*, *Neurog2*, *Hes6*), bipolar cell specification (*Otx2*), or otherwise broadly neurogenesis (*Insm1*, *Dll3*, *Mybl1*) or are selectively expressed in late-stage neurogenic progenitors in the developing retina (*Gadd45a*, *Btg2*) (Clark et al., 2019) (Fig. 3e,f, Table ST1). These findings imply that Oct4 enhances bipolar cell formation in *Rbpj*-deficient Müller glia potentially by repressing expression of genes that promote quiescence such as *Lhx2* (de Melo et al., 2018, 2016), increasing expression of genes that broadly promote neurogenesis, and selectively increasing expression of the bipolar cell-promoting factor *Otx2* (Chan et al., 2020; Wang et al., 2014).

Single-cell multiomic analysis identifies targets of Oct4 in wildtype and *Rbpj*-deficient Müller glia

To further investigate the mechanism by which Oct4 promotes neurogenesis, we conducted simultaneous single-nucleus (sn)RNA-Seq and ATAC-Seq on GFP-positive cells from both wildtype and *Rbpj*-deficient Müller glia infected with either control or Oct4-mCherry vectors at 8 weeks following NMDA injection (Fig. 4a). UMAP analysis of integrated cellular snRNA/ATAC-Seq profiles was then used to identify cell clusters. Müller glia from wildtype and *Rbpj*-deficient animals form two separate Müller glia clusters (Fig. 4b,c). AAV-infected wildtype Müller glia could be readily identified by selective expression of Oct4 (Fig.4e). Wildtype Oct4-expressing Müller glia give rise to both small numbers of neurogenic MGPCs (Fig. 4b), in line with the small numbers of Ascl1-positive cells observed (Fig. S2g,h), as well as mature bipolar cells, consistent with histological findings (Fig. 1c,d). Oct4 overexpression substantially enhances bipolar cell generation from *Rbpj*-deficient MGPC (Fig. 4d, Fig. S8). Although small numbers of rod and cone photoreceptors are detected in this analysis, their proportions do not substantially change between treatment conditions, and therefore likely represent cellular contaminants.

Oct4 overexpression leads to significant changes in gene expression in both wildtype and *Rbpj*-deficient Müller glia. The transition from resting to neurogenic MGPCs to bipolar cells is associated with downregulation of genes that are specifically expressed in resting Müller glia, including *Aqp4, Hes1, Tcf7l2,* and *Lhx2* (Fig. 4e,f, Table ST2). Similarly, motif analysis showed that chromatin accessibility is reduced for target motifs for transcription factors that maintain glial quiescence such as Nfia/b/x and Lhx2 (Fig. 4g, Fig. S8, Table ST2). MGPCs likewise show increased accessibility at Stat1/3 motifs, as well as target motifs for neurogenic transcription

factors such as Ascl1, Neurog2, and Neurod1 (Fig. 4g), consistent with previous studies of MGPCs generated from *Nfia/b/x* and *Rbpj*-deficient Müller glia (Hoang et al., 2020; Le et al., 2024).

Oct4 overexpression in both wildtype and *Rbpj*-deficient Müller glia clusters respectively induces upregulation of 534 and 1657 genes, while respectively downregulating 439 and 824 genes (Fig. 4h). A total of 156 genes are upregulated in both wildtype and *Rbpj*-deficient Müller glia, while 63 genes are downregulated. In both wildtype and *Rbpj*-deficient Müller glia, Oct4 upregulates multiple classes of ion channels, including mechanosensitive (*Piezo2*), TRP (*Trpm*1, *Trpm3*), and chloride channels (*Clca3a1*, *Clca3a2*), as well as GABA receptors (*Gabra4*, *Gabrb1*), cyclic nucleotide phosphodiesterases (*Pde8b*, *Pde11a*), and the neuropeptide *Npy*. *Oct4* overexpression also selectively downregulates multiple inflammation-associated genes *(B2m*, *H2-D1*), small GTPases (*Gbp2*, *Igtp*, *Irgm2*, *Rab13*, *Rgs20*, *Tgtp2*), along with the glycolytic enzyme *Gapdh* and many ribosomal subunits (Fig. 4h, Table ST3). This functionally diverse range of genes that are not prominently expressed in retinal progenitors, and whose role in controlling neurogenic competence remains to be investigated.

Oct4 also differentially regulates multiple transcription factors in both wildtype and *Rbpj*-deficient Müller glia. As expected, *Pou5f1* mRNA is strongly upregulated (Fig. 4e,h), with increased chromatin accessibility also being observed at the endogenous *Pou5f1* promoter, indicating that Oct4 regulates its self-expression (Fig. 4i, Table ST4). Similarly, *Oct4* overexpression strongly upregulates the transcription factor *Rfx4* and accessibility at its endogenous promoter (Fig. 4e,h,i, Table ST4). Overexpression of *Rfx4* is sufficient to induce neurogenesis when overexpressed in human embryonic stem cells (Choi et al., 2024; Joung et al., 2024). However, *Rfx4* is not detectably expressed in developing mouse retinas (Clark et al., 2019), indicating that Oct4-induced neurogenesis may involve mechanisms beyond simply inducing dedifferentiation to a retinal progenitor-like state.

Several other transcription factors are only differentially regulated following *Oct4* overexpression in *Rbpj*-deficient Müller glia. One notable upregulated transcription factor is Klf4, which cooperates with Oct4 to induce pluripotency (Takahashi and Yamanaka, 2006). In contrast, Stat1, which inhibits neurogenesis induced by Ascl1 overexpression in Müller glia (Jorstad et al., 2020), is selectively downregulated in *Rbp*j-deficient Müller glia (Fig. 4h, Table ST3).

Analysis of changes in chromatin accessibility induced by Oct4 reveals that the consensus motif for Oct4 and its close variant Pit1 (Pou1f1) show the strongest increase in accessibility, followed by Rfx family motifs (Fig. 4j,Table ST5). Both wildtype and *Rbpj*-deficient Müller glia show increased accessibility associated with Sox2, which directly interacts with Oct4 and cooperates to induce pluripotency (Rizzino, 2013). While Oct4 does not significantly upregulate the pluripotency factor *Klf4* in wildtype Müller glia, it robustly induces *Klf4* expression *Rbpj*-deficient Müller glia, and likewise selectively induces accessibility at Klf4 consensus motif sites (Fig. 4j). In addition, *Rbpj*-deficient Müller glia also show smaller but still significant increases in accessibility at target sites for the proneural factor Neurog2 and the neurogenic

factor Insm1 (Lyu et al., 2021), identifying additional mechanisms by which Oct4 might synergistically enhance neurogenesis (Fig. 4j, Table ST5).

Discussion:

In this study, we demonstrate that AAV-mediated overexpression of Oct4 is sufficient to induce neurogenic competence in wildtype Müller glia in adult mice, and to synergistically enhance neurogenesis induced by genetic disruption of Notch signaling. While Oct4 overexpression induces very low levels of proliferation, Oct4-induced neurogenesis appears to mostly result from direct glia-to-bipolar cell transdifferentiation by simultaneously upregulating expression of neurogenic bHLH factors and the bipolar cell promoting factor *Otx2*. In addition, Oct4 upregulates expression of the neurogenic transcription factor *Rfx4*, which is not expressed during retinal development. Oct4 exerts reprogramming effects by broadly increasing chromatin accessibility at predicted regulatory sites associated with these genes.

While we did not detect endogenous *Oct4* expression in either injured or neurogenic mouse Müller glia, the fact that these cells express robust levels of *Sox2*, *Klf4*, and *Myc* implies that they may already be prime to reprogramming induced by Oct4. Our findings differ from two previous reports that initially motivated us to carry out this study. A previous study in zebrafish showed weak levels of the Oct4 homolog *pou5f3* in resting glia, with these levels increasing dramatically following injury (Sharma et al., 2019). It remains unclear why we were unable to detect more than trace levels of *pou5f3* expression in zebrafish Müller glia in any of the many bulk and single-cell RNA-Seq samples we analyzed (Hoang et al., 2020). We also did not detect the previously reported low levels of injury-induced *Oct4* expression in mouse Müller glia (Reyes-Aguirre and Lamas, 2016). Similar discrepancies in observed cellular patterns of *Oct4* expression have been observed in many other tissues (Lengner et al., 2008), and further work will be needed to clarify these discrepancies.

This study represents a clear instance in which viral-mediated expression coupled with genetic cell lineage analysis was effectively used to induce the conversion of adult mammalian Müller glia into retinal neurons *in situ*. A similar approach has been also successfully used to generate bipolar neurons from both immature (Pollak et al., 2013) and very recently also in mature, Müller glia by overexpression of the neurogenic bHLH factors *Ascl1* and *Atoh1* (Pavlou et al., 2024). Other studies reported efficient conversion of Müller glia to photoreceptors using a complex cocktail of overexpressed factors, including *Ctnnb1*, *Otx2*, *Crx*, and *Nrl* (Yao et al., 2018), and efficient conversion of Müller glia to retinal ganglion cells following overexpression of *Atoh7* and *Pou4f2* (Xiao et al., 2021). However, these studies both used GFAP minipromoters to both drive expression of these constructs and to infer cell lineage. Multiple studies have shown that GFAP minipromoter specificity is heavily influenced by insert sequences present in AAVs, which can result in both silencing of expression in glia and ectopic activation of expression in neurons (Le et al., 2022; L.-L. Wang et al., 2021). As a result, it cannot be concluded that these represent bona fide glia-to-neuron conversion *in vivo*. Similar claims have been made about knockdown of the RNA binding protein *Ptbp1*, which was variously claimed to directly convert Müller glia to either retinal ganglion cells or photoreceptors, but has been debunked using genetic cell lineage analysis (Hoang et al., 2022; Xie et al., 2022). In this study, the combination

of prospective cell lineage analysis using the *GlastCreER;Sun1-GFP* transgene before infection with GFAP-Oct4-mCherry vector, in combination with scRNA-Seq analysis of infected cells, rules out any potentially confounding factors resulting from the GFAP minipromoter.

Our finding that Oct4 can synergistically enhance neurogenesis induced by genetic disruption of Notch signaling raises the question of whether this might be more broadly applicable to other models of induced neurogenesis in mammalian Müller glia. The mechanism by which Oct4 induces glial-derived neurogenesis appears complex, and to differ fundamentally from that seen following either overexpression of *Ascl1* or loss of function of *Nfia/b/x* and/or *Rbpj* (Hoang et al., 2020; Jorstad et al., 2017; Le et al., 2024). In these cases, Müller glia broadly upregulate proneural genes and/or downregulate Notch signaling. Oct4 instead induces expression of the neurogenic transcription factor *Rfx4*, which is not expressed in developing retina. It is likely that activation of this parallel pathway to neurogenic competence in part accounts for synergistic induction of neurogenesis seen in *Rbpj*-deficient Müller glia.

Other mechanisms enhancing Oct4-dependent neurogenesis in the *Rbpj*-deficient Müller glia may include enhanced induction of *Klf4* expression and increased accessibility at target sites for neurogenic transcription factors such as Ascl1. While *Ascl1* overexpression induces Müller glia-derived neurogenesis in adult mice, this occurs only following treatment with HDAC inhibitors (Jorstad et al., 2017), even though Ascl1 is itself a pioneer factor (Păun et al., 2023). *Oct4* overexpression broadly increases the accessibility of putative cis-regulatory sequences associated with both *Neurog2* and *Insm1*, identifying another potential mechanism of synergy. Transient overexpression of Oct4 could potentially further enhance the neurogenic function of Ascl1 and enhance glial-derived neurogenesis more broadly. This may also be the case for pathways reported to induce glial reprogramming in other CNS regions, such as *Sox2* overexpression (Niu et al., 2015). Since *Oct4* overexpression only weakly and transiently induces proliferation in adult Müller glia, this reduces the potential oncogenic risk, and may ultimately prove to be relevant for the design of cell-based regenerative therapies for treating retinal dystrophies.

Methods:

Mice

Mice were raised and housed in a climate-controlled pathogen-free facility on a 14/10 h light/dark cycle. Mice used in this study were *GlastCreER;Sun1-GFP*, which were generated by crossing the *GlastCreER* and *Sun1-GFP* lines developed by Dr. Jeremy Nathans at Johns Hopkins (de Melo et al., 2012; Mo et al., 2015), and were obtained from his group. *GlastCreER*;*Rbpj*$^{lox/lox}$*;Sun1-GFP* mice were generated by crossing *GlastCreER;Sun1GFP* with conditional *Rbpj*$^{lox/lox}$ *mice* (JAX #034200).
GlastCreER;*Notch1*$^{lox/lox}$*;Notch2*$^{lox/lox}$*;Sun1-GFP* mice were obtained by crossing *GlastCreER*;*Notch1*$^{lox/lox}$*;Sun1-GFP* and *GlastCreER*;*Notch2*$^{lox/lox}$*;Sun1-GFP* mice.
GlastCreER;*Nfia/b/x*$^{lox/lox}$;*Sun1-GFP* mice were generated by crossing *Nfia*$^{lox/lox}$(*see* below); *Nfib*$^{lox/lox}$ (Hsu et al., 2011), and *Nfix*$^{lox/lox}$ (Campbell et al., 2008) mice to *GlastCreER;Sun1-GFP* mice. *Nfia*$^{lox/lox}$ mice were generated in the Roswell Park Gene Targeting and Transgenic Shared Resource using heterozygous targeted ES cells from EUCOMM project 38437 (KOMP).

Maintenance and experimental procedures performed on mice were in accordance with the protocol approved by the Institutional Animal Care and Use Committee (IACUC) at the Johns Hopkins School of Medicine.

Intraperitoneal tamoxifen (TAM) Injection

To induce *Cre* recombination, animals at ~3 weeks of age were intraperitoneally injected with tamoxifen (Sigma-Aldrich, #H6278-50mg) in corn oil (Sigma-Aldrich, #C8267-500ML) at 1.5mg/dose for five consecutive days.

NMDA treatment

Adult mice were anesthetized with isoflurane inhalation. Two microliters of 100 mM NMDA in PBS were intravitreally injected using a microsyringe with a 33G blunt-ended needle.

EdU treatment

At 1-week post tamoxifen induction, mice were administered EdU (Abcam, #ab146186) via i.p. injections (150µl of 5mg/ml in PBS) and drinking water (0.3 mg/ml) for 7 consecutive days.

Cloning, production, and intravitreal injection of Adeno-Associated Virus

The Addgene #50473 construct which contains a GFAP promoter was used in this study. The EGFP sequence was replaced by the mCherry sequence. The P2A ribosomal self-cleaving peptide is used to simultaneously express *Oct4* 5′ to the mCherry reporter as a single polypeptide, which is then cleaved to generate *Oct4* and mCherry. The coding sequence of *Oct4* was synthesized by GeneWiz. AAV constructs were packaged into AAV2.7m8 by Boston Children's Hospital Viral Core. Following tam induction, one-month-old GlastCreER;Sun1-GFP mice were intravitreally injected with GFAP AAV constructs using a microsyringe with a 33G blunt-ended needle. The titres and injection volume for each construct are listed in table ST6.

Immunohistochemistry and imaging

Collection and immunohistochemical analysis of retinas were performed as described previously (Hoang et al., 2020). Mouse eye globes were fixed in 4% paraformaldehyde (ElectronMicroscopySciences, #15710) for 4 h at 4°C. Retinas were dissected in 1x PBS and incubated in 30% sucrose overnight at 4°C. Retinas were then embedded in OCT (VWR, #95057-838), cryosectioned at 16 µm thickness, and stored at −20°C. Sections were dried for 30 min in a 37°C incubator and washed 3 × 5 min with 0.1% TritonX-100 in PBS (PBST). EdU labeling was performed by using Click-iT EdU kit (ThermoFisher, #C10340, #C10636) following the manufacturer's instructions. Sections were then incubated in blocking buffer (10% Horse Serum (ThermoFisher, #26050070), 0.4% TritonX-100 in 1x PBS) for 2 h at room temperature (RT) and then incubated with primary antibodies in the blocking buffer overnight at 4°C. Primary antibodies used are listed in Table ST7.

Sections were washed 4 x 5 min with PBST to remove excess primary antibodies and were incubated in secondary antibodies in blocking buffer for 2 h at RT. Sections were then counterstained with DAPI in PBST, washed 4 x 5 min in PBST and mounted with ProLong Gold Antifade Mountant (Invitrogen, #P36935) under coverslips (VWR, #,48404-453), air-dried, and

stored at 4°C. Fluorescent images were captured using a Zeiss LSM 700 confocal microscope. Secondary antibodies used are listed in table ST7.

Cell quantification and statistical analysis

Otx2/GFP-positive and HuC/D/GFP-positive cells were counted and divided by the total number of GFP-positive cells from a single random whole section per retina. Each data point in the bar graphs was calculated from an individual retina. All cell quantification data were graphed and analyzed using GraphPad Prism 10. Two-way ANOVA was used for analysis between 3 or more samples of multiple groups. All results are presented as mean ± SD.

Retinal cell dissociation

Retinas were dissected in fresh ice-cold PBS and retinal cells were dissociated using an optimized protocol as previously described (Fadl et al., 2020). Each sample contains a minimum of 4 retinas from 4 animals of both sexes. Dissociated cells were resuspended in ice-cold HBAG Buffer containing Hibernate A (BrainBits, #HALF500), B-27 supplement (ThermoFisher, #17504044), and Glutamax (ThermoFisher, #35050061).

Single-cell RNA-sequencing (scRNA-seq) library preparation

scRNA-seq were prepared on dissociated retinal cells using the 10X Genomics Chromium Single Cell 3' Reagents Kit v3.1 (10X Genomics, Pleasanton, CA). Libraries were constructed following the manufacturer's instructions and were sequenced using Illumina NextSeq. Sequencing data were processed through the Cell Ranger 7.0.1 pipeline (10X Genomics) using default parameters.

Single-cell Multiome ATAC + GEX sequencing library preparation

scATAC-seq and scRNA-seq were prepared on FACS-isolated GFP-positive cells using the 10X Genomic Chromium Next GEM Single Cell Multiome ATAC + Gene Expression kit following the manufacturer's instructions. Briefly, cells were spun down at 500xg for 5 min, resuspended in 100 µl of ice-cold 0.1x Lysis Buffer, lysed by pipette-mixing 4 times, and incubated on ice for 4 min total. Cells were washed with 0.5 ml of ice-cold Wash Buffer and spun down at 500xg for 5 min at 4°C. Nuclei pellets were resuspended in 10-15 µl Nuclei Buffer and counted using Trypan blue. Resuspended cell nuclei (10-15k) were utilized for transposition and loaded into the 10x Genomics Chromium Single Cell system. ATAC libraries were amplified with 10 PCR cycles and were sequenced on Illumina NovaSeq with ~200 million reads per library. RNA libraries were amplified from cDNA with 14 PCR cycles and were sequenced on Illumina NovaSeq 6000

scRNA-seq data analysis

ScRNA-Seq data were pre-processed using Cellranger v7.1.0 using custom mouse genome mm10 with mCherry and Sun1GFP sequences. The cell-by-genes count matrices were further analyzed using Seurat V5.1.0 (Hao et al., 2024).Cells with RNA counts less than 1000 or greater than 25,000, and number of genes less than 500 or greater than 6000 were filtered out as low-quality cells. Additionally, cells with a mitochondrial fraction of greater than 10% were removed. For data visualization, UMAP was generated using the first 20 dimensions. Müller glia

and MGPC cell clusters were subsetted for further analysis. Differential gene expression of mCherry control and Oct4-mCherry groups was performed using “FindAllMarkers” function.

Single-cell Multiomic analysis

For the data processing, raw scRNA-seq and scATAC-seq data were processed with the Cell Ranger software version 2.0.2 specifically using cellranger-arc pipeline for formatting reads, demultiplexing samples, genomic alignment, and generating the cell-by-gene count matrix and the fragments files. Both the cell-by-gene count matrix and the fragments files are the final output from the cellranger-arc pipeline and were used for all downstream analysis.

For data analysis, scRNA-seq and scATAC-seq were analyzed using Archr version 1.0.2. EnsDb.Mmusculus.v79 and BSgenome.Mmusculus.UCSC.mm10 were used for annotations. The arrow file for each sample was created using the cell-by-gene count matrix and the fragments files output from the cellranger-arc pipeline. To filter poor quality cells, Gex_nGenes greater than 500 and less than 5000 were kept, Gex_nUMI greater than 1000 and less than 15,000 were kept. Also, TSSEnrichment greater than 10 and nFrags greater than 5000 were kept, other cells were deemed of poor quality and were filtered out. Gene expression values from a paired scATAC-seq and scRNA-seq multi modal assay were added to the arrow files using “addGeneExpressionMatrix” function. The LSI dimensionality reduction for both scATAC and scRNASeq was computed and combined using the “addCombinedDims” function. UMAP embedding is calculated using “addUMAP” function and clusters are identified from the reduced dimensions. Marker features were used to annotate clusters.

To obtain peaks, “addReproduciblePeakSet” function was used to get insertions from coverage files, call peaks, and merge peaks and this step internally used macs software. Then the “addPeakMatrix” function was called to independently compute counts for each peak per cell. To link peaks to genes, “getPeak2GeneLinks” function was called. The “getMarkerFeatures” function was used to get the differential gene expressions and the differential peaks expressions using the GeneExpressionMatrix and PeakMatrix calculated respectively. Peaks with motifs were annotated using the cisbp motif set using “annotatePeaks.pl” from HOMMER version 4.11 to associate the peaks with nearby genes. Full code used for the analysis is available at https://github.com/SherineAwad/OCT4scRNA-ATAC

Funding: This study was supported by an award from the National Eye Institute (R01EY031685) to S.B., a Stein Innovation Award from Research to Prevent Blindness to S.B., and a Young Investigator grant from Alcon Research Institute to T.H.

Author contributions: N.L. collected and analyzed the bulk of all data presented here. S.A. analyzed single-cell multiomic data, and I.P. assisted in generating multiomic data. T.H. initiated the study, and collected pilot data. S.B. supervised, coordinated, and directed this work. N.L., T.H., and S.B. drafted the manuscript, which all authors edited.

Declaration of interests: S.B. is a co-founder and shareholder of CDI Labs, LLC, and receives support from Genentech.

Data and materials availability: All scRNA-seq, snRNA-seq, and scATAC-seq data described in this study are available at Gene Expression Omnibus under accession number GSE277390.

Figure legends:

Figure 1: AAV-mediated overexpression of *Oct4* induces neurogenesis in wildtype mouse Müller glia following NMDA-induced excitotoxicity. (A) Schematic of the transgenic construct used to specifically label Müller glia with Sun1-GFP expression. **(B)** Schematic of the GFAP AAV constructs and experimental workflow. **(C)** Representative images of retinas immunolabeled for GFP, mCherry, Otx2, and HuC/D. White arrowheads indicate GFP-positive Müller glia-derived neurons expressing neuronal markers Otx2 or HuC/D. **(D)** Quantification of mean percentage ± SD of GFP-positive Müller glia-derived neurons expressing either Otx2 or HuC/D. Significance was determined via two-way ANOVA with Tukey's multiple comparison test: ****$p < 0.0001$. Each data point was calculated from an individual retina. TAM, tamoxifen; ONL, outer nuclear layer; INL, inner nuclear layer; GCL, ganglion cell layer. Scale bar = 50μm.

Figure 2: *Oct4* overexpression enhances neurogenesis observed in *Rbpj*-deficient Müller glia. (A) Schematic of the transgenic constructs used to induce loss of function of *Rbpj* specifically in Müller glia. **(B)** Schematic of the GFAP AAV constructs and experimental workflow. **(C)** Representative images of retinas immunolabeled for GFP, mCherry, Otx2, and HuC/D. White arrowheads indicate GFP-positive Müller glia-derived neurons expressing neuronal markers Otx2 or HuC/D. **(D)** Quantification of mean percentage ± SD of GFP-positive Müller glia-derived neurons expressing either Otx2 or HuC/D. Significance was determined via two-way ANOVA with Tukey's multiple comparison test: ****$p < 0.0001$. TAM, tamoxifen; ONL, outer nuclear layer; INL, inner nuclear layer; GCL, ganglion cell layer. Scale bar = 50μm.

Figure 3: ScRNA-Seq analysis of Müller glia and Müller glia-derived neurons derived from *Rbpj*-deficient Müller glia following *Oct4* overexpression. **(A)** Schematic of the scRNA-seq experimental pipeline. **(B)** UMAP plot showing the clustering of GFP-positive cells from retinas infected with GFAP-mCherry and GFAP-Oct4-mCherry AAV constructs. **(C)** Stacked bar plots showing the proportion of cells in each cluster across two sample groups. **(D)** Feature plots highlighting the cluster of Müller glia (*Hes5*), neurogenic MGPCs (*Neurog2, Insm1, Ascl1*), bipolar cells (*Otx2*), and amacrine cells (*Elavl3*). **(E)** Heatmap showing the expression of top differentially expressed genes (DEGs) for *Rbpj*-deficient Müller glia cell cluster from retinas infected with GFAP-mCherry and GFAP-Oct4-mCherry AAV constructs. **(F)** Heatmap showing the expression of top differentially expressed genes (DEGs) for MGPC cell cluster from retinas infected with GFAP-mCherry and GFAP-Oct4-mCherry AAV constructs.

Figure 4: Integrated snRNA/scATAC-Seq analysis of control and *Rbpj*-deficient Müller glia with *Oct4* overexpression. (A) Schematic of the multiomic scRNA/ATAC-seq experimental pipeline. **(B)** UMAP plot of multiomic datasets showing the clustering of GFP+ cells from control and *Rbpj*-deficient Müller glia from GFAP-mCherry and GFAP-Oct4-mCherry AAV infected retinas. **(C)** UMAP plot showing the identity of cell clusters determined by marker gene expression. **(D)** Stacked bar plots represent the proportion of cells in each cluster across different sample groups. **(E)** Feature plots highlighting the cluster of Müller glia (*Hes1*), neurogenic MGPCs (*Neurog2, Sox4*), bipolar cells (*Otx2*), *Pou5f1*- and *Rfx4*-expressing cells. **(F)** Heatmap showing expression of DEGs along the neurogenesis trajectory. (**G**) Heatmap showing differential motif activity along the neurogenesis trajectory. (**H**) Heatmaps of DEGs

differentially expressed between Oct4 and mCherry control samples in the wildtype and *Rbpj*-deficient Müller glia cell clusters. Venn diagram showing unique and common DEGs between Oct4 and mCherry control in the wildtype and *Rbpj*-deficient Müller glia clusters. (**I)** Increased chromatin accessibility regions associated with the *Oct4* and *Rfx4* loci observed following *Oct4* overexpression in both wildtype and *Rbpj*-deficient Müller glia. (**J**) Top-ranked enriched motifs in chromatin regions showing increased accessibility following *Oct4* overexpression in both wildtype and *Rbpj*-deficient Müller glia cell clusters.

Figure S1: *Oct4/pou5f3* mRNA is not detectably expressed in Müller glia after injury. Expression of pluripotency factors in resting or injured retinas by scRNA-Seq and bulk RNA data in (**a**) zebrafish and (**b**) mouse after retinal injury from Hoang et al., 2020 and in (**c**) *Nfia/b/x;Rbpj*-deficient Müller glia from Le et al., 2024.

Figure S2: Immunohistochemical analysis of glial, AAV reporter, and additional molecular markers at 1- and 2-weeks following NMDA in wildtype Müller glia. (a) Schematic of the transgenic construct used to specifically label Müller glia with Sun1-GFP expression. **(b)** Schematic of the GFAP AAV constructs and experimental workflow. Representative images of retinas immunolabeled for GFP, mCherry and **(c-d)** Sox2, (**e-f**) EdU/Iba1, (**g-h**) Ascl1, (**i-j**) Oct4, (**k-l**) Otx2. White arrowheads indicate GFP-positive cells expressing selected markers. Yellow arrowheads indicate GFP-positive cells that do not co-label with Sox2 and EdU/Iba1+ cells that do not co-label with GFP+ cells. Quantification of mean percentage ± SD of GFP-positive Müller glia co-labeled with (**m**) EdU and (**n**) Otx2 . Significance was determined via two-way ANOVA with Tukey's multiple comparison test: ***$p < 0.001$, *$p < 0.05$. Each data point was calculated from an individual retina. TAM, tamoxifen; ONL, outer nuclear layer; INL, inner nuclear layer; GCL, ganglion cell layer. Scale bar = 50μm.

Figure S3: Immunohistochemical analysis of glial, AAV reporter, and additional molecular markers of Müller glia-derived neurons at 5 weeks following NMDA following *Oct4* transduction in wildtype and *Rbpj*-deficient Müller glia. (**a**-**h**) Representative images of wildtype retina immunolabeled for GFP, mCherry, and (**a**) Oct4, (**b**) Ascl1, (**c**) Sox2, (**d**) Scgn, (**e**) Cabp5, (**f**) Isl1, (**g**) Nrl, (**h**) EdU. (**i-k**) Representative images of Rbpj cKO retina immunolabeled for GFP, mCherry, and (**i**) Oct4, (**j**) Sox9, (**k**) EdU. White arrowheads indicate GFP-positive cells co-labeled with the relevant marker. Yellow arrowheads indicate GFP-positive Müller glia that did not co-labeled with Müller glia markers. ONL, outer nuclear layer; INL, inner nuclear layer; GCL, ganglion cell layer. Scale bar = 50μm.

Figure S4: Immunohistochemical analysis of glial, AAV reporter, and additional molecular markers at 1- and 2-weeks following NMDA in *Rbpj*-deficient Müller glia. (a) Schematic of the transgenic constructs used to induce loss of function of *Rbpj* specifically in Müller glia. **(b)** Schematic of the GFAP AAV constructs and experimental workflow. Representative images of retinas immunolabeled for GFP, mCherry and **(c-d)** Sox2, (**e-f**) EdU/Iba1, (**g-h**) Ascl1, (**i-j**) Oct4, (**k-l**) Otx2. White arrowheads indicate GFP-positive cells expressing selected markers. Yellow arrowheads indicate GFP-positive cells that do not co-label with Sox2 and EdU/Iba1+ cells that do not co-label with GFP+ cells. **(m)** Quantification of

mean percentage ± SD of GFP-positive Müller glia-derived neurons expressing Otx2. Significance was determined via two-way ANOVA with Tukey's multiple comparison test: *p < 0.05. Each data point was calculated from an individual retina. TAM, tamoxifen; ONL, outer nuclear layer; INL, inner nuclear layer; GCL, ganglion cell layer. Scale bar = 50μm.

Figure S5: AAV-mediated overexpression of *Oct4* induces neurogenesis in injured *Notch1/2*-deficient Müller glia. (**a**) Schematic of the transgenic mice used to induce deletion of *Notch1/2* specifically in Müller glia. (**b**) Schematic of the experimental workflow. (**c**) Representative images of retinas immunolabeled for GFP, mCherry, Otx2, and HuC/D. White arrowheads indicate GFP-positive Müller glia-derived neurons expressing neuronal markers Otx2 or HuC/D. Quantification of mean percentage ± SD of GFP-positive Müller glia-derived neurons expressing either Otx2 or HuC/D. Significance was determined via two-way ANOVA with Tukey's multiple comparison test: ****p < 0.0001. TAM, tamoxifen; ONL, outer nuclear layer; INL, inner nuclear layer; GCL, ganglion cell layer. Scale bar = 50μm.

Figure S6: *Oct4* overexpression does not enhance neurogenesis in *Nfia/b/x*-deficient Müller glia because GFAP minipromoter is not active in these cells. (**a**) Schematic of the transgenic mice used to induce deletion of *Nfia/b/x* specifically in Müller glia. (**b**) Schematic of the experimental workflow. (**c**) Representative images of retinas immunolabeled for GFP, mCherry, Otx2, and HuC/D. White arrowheads indicate mCherry expression in Sox2+ Müller glia that are not Sun1-GFP+. Quantification of mean percentage ± SD of GFP-positive Müller glia-derived neurons expressing either Otx2 or HuC/D. TAM, tamoxifen; ONL, outer nuclear layer; INL, inner nuclear layer; GCL, ganglion cell layer. Scale bar = 50μm.

Figure S7: ScRNA-Seq analysis of Müller glia-derived neurons from *Rbpj*-deficient Müller glia following *Oct4* overexpression. (a**)** UMAP plot showing GFP-positive cells from retinas infected with GFAP-mCherry and GFAP-Oct4-mCherry AAVs. (**b**) Expression of glial and neuronal markers. (**c**) Top DEGs of different cell types generated by Oct4 overexpression in Rbpj cKO.

Figure S8: Pseudotime analysis showing the transition from resting to neurogenic MGPCs to bipolar cells. (**a**) Top DEGs across different retinal cell types. (**b**) Pseudotime trajectory of neurogenesis from Müller glia to bipolar cells. (**c**) Heatmap showing differential chromatin accessible regions at different pseudotime stages along the neurogenesis trajectory.

Table ST1: ScRNA-Seq analysis of Sun1-GFP Müller glia-derived cells identifies genes differentially regulated by *Oct4* overexpression. Raw+adjusted p-values, relative fold-change, and the fraction of all profiled cells expressing the gene in question is shown for both Muller glia and Muller glia-derived progenitor cells transfected with AAV-GFAP-Oct4-mCherry vs. AAV-GFAP-mCherry.

Table ST2: Multiomic analysis identifies DEGs, differential chromatin accessible regions and differentially accessible transcription factor target motifs are shown at discrete pseudotime intervals along the Müller glia-bipolar differentiation trajectory.

Table ST3: SnRNA-Seq analysis identifies DEGs induced by Oct4 overexpression from wildtype and *Rbpj*-deficient Müller glia cell clusters.

Table ST4: SnATAC-Seq analysis identifies differentially accessible chromatin regions regulated by *Oct4* overexpression in wildtype and *Rbpj*-deficient Müller glia cell clusters.

Table ST5: SnATAC-Seq analysis identifies differential motif activity in increased accessible chromatin regions by Oct4 overexpression in wildtype and *Rbpj*-deficient Müller glia cell clusters.

Table ST6: List of AAV constructs used in the study. Columns identify the AAV construct, titre, and injection volume.

Table ST7: List of antibodies used in the study. Columns identify the antibody, source, catalog number, and RRID identifier.

References:

Abad M, Mosteiro L, Pantoja C, Cañamero M, Rayon T, Ors I, Graña O, Megías D, Domínguez O, Martínez D, Manzanares M, Ortega S, Serrano M. 2013. Reprogramming in vivo produces teratomas and iPS cells with totipotency features. *Nature* **502**:340–345.

Asadi S, Dehghan S, Hajikaram M, Mowla SJ, Ahmadiani AA, Javan M. 2015. Comparing The Effects of Small Molecules BIX-01294, Bay K8644, RG-108 and Valproic Acid, and Their Different Combinations on Induction of Pluripotency Marker-Genes by Oct4 in The Mouse Brain. *Cell J* **16**:416–425.

Campbell CE, Piper M, Plachez C, Yeh Y-T, Baizer JS, Osinski JM, Litwack ED, Richards LJ, Gronostajski RM. 2008. The transcription factor Nfix is essential for normal brain development. *BMC Dev Biol* **8**:52.

Cebolla B, Vallejo M. 2006. Nuclear factor-I regulates glial fibrillary acidic protein gene expression in astrocytes differentiated from cortical precursor cells. *J Neurochem* **97**:1057–1070.

Chan CSY, Lonfat N, Zhao R, Davis AE, Li L, Wu M-R, Lin C-H, Ji Z, Cepko CL, Wang S. 2020. Cell type- and stage-specific expression of Otx2 is regulated by multiple transcription factors and -regulatory modules in the retina. *Development* **147**. doi:10.1242/dev.187922

Choi W, Choe MS, Kim SM, Kim SJ, Lee J, Lee Y, Lee S-M, Dho SH, Lee M-Y, Kim LK. 2024. RFX4 is an intrinsic factor for neuronal differentiation through induction of proneural genes POU3F2 and NEUROD1. *Cell Mol Life Sci* **81**:99.

Clark BS, Stein-O'Brien GL, Shiau F, Cannon GH, Davis-Marcisak E, Sherman T, Santiago CP, Hoang TV, Rajaii F, James-Esposito RE, Gronostajski RM, Fertig EJ, Goff LA, Blackshaw S. 2019. Single-Cell RNA-Seq Analysis of Retinal Development Identifies NFI Factors as Regulating Mitotic Exit and Late-Born Cell Specification. *Neuron* **102**:1111–1126.e5.

Dehghan S, Asadi S, Hajikaram M, Soleimani M, Mowla SJ, Fathollahi Y, Ahmadiani A, Javan M. 2015. Exogenous Oct4 in combination with valproic acid increased neural progenitor markers: an approach for enhancing the repair potential of the brain. *Life Sci* **122**:108–115.

Dehghan S, Hesaraki M, Soleimani M, Mirnajafi-Zadeh J, Fathollahi Y, Javan M. 2016. Oct4 transcription factor in conjunction with valproic acid accelerates myelin repair in demyelinated optic chiasm in mice. *Neuroscience* **318**:178–189.

de Melo J, Clark BS, Venkataraman A, Shiau F, Zibetti C, Blackshaw S. 2018. Ldb1- and Rnf12-dependent regulation of Lhx2 controls the relative balance between neurogenesis and gliogenesis in the retina. *Development* **145**. doi:10.1242/dev.159970

de Melo J, Miki K, Rattner A, Smallwood P, Zibetti C, Hirokawa K, Monuki ES, Campochiaro PA, Blackshaw S. 2012. Injury-independent induction of reactive gliosis in retina by loss of function of the LIM homeodomain transcription factor Lhx2. *Proc Natl Acad Sci U S A* **109**:4657–4662.

de Melo J, Zibetti C, Clark BS, Hwang W, Miranda-Angulo AL, Qian J, Blackshaw S. 2016. Lhx2 Is an Essential Factor for Retinal Gliogenesis and Notch Signaling. *J Neurosci* **36**:2391–2405.

Fadl BR, Brodie SA, Malasky M, Boland JF, Kelly MC, Kelley MW, Boger E, Fariss R,

Swaroop A, Campello L. 2020. An optimized protocol for retina single-cell RNA sequencing. *Mol Vis* **26**:705–717.
Gao X, Wang X, Xiong W, Chen J. 2016. In vivo reprogramming reactive glia into iPSCs to produce new neurons in the cortex following traumatic brain injury. *Sci Rep* **6**:22490.
Hao Y, Stuart T, Kowalski MH, Choudhary S, Hoffman P, Hartman A, Srivastava A, Molla G, Madad S, Fernandez-Granda C, Satija R. 2024. Dictionary learning for integrative, multimodal and scalable single-cell analysis. *Nat Biotechnol* **42**:293–304.
Hoang T, Kim DW, Appel H, Pannullo NA, Leavey P, Ozawa M, Zheng S, Yu M, Peachey NS, Blackshaw S. 2022. Genetic loss of function of Ptbp1 does not induce glia-to-neuron conversion in retina. *Cell Rep* **39**:110849.
Hoang T, Wang J, Boyd P, Wang F, Santiago C, Jiang L, Yoo S, Lahne M, Todd LJ, Jia M, Saez C, Keuthan C, Palazzo I, Squires N, Campbell WA, Rajaii F, Parayil T, Trinh V, Kim DW, Wang G, Campbell LJ, Ash J, Fischer AJ, Hyde DR, Qian J, Blackshaw S. 2020. Gene regulatory networks controlling vertebrate retinal regeneration. *Science* **370**. doi:10.1126/science.abb8598
Hsu Y-C, Osinski J, Campbell CE, Litwack ED, Wang D, Liu S, Bachurski CJ, Gronostajski RM. 2011. Mesenchymal nuclear factor I B regulates cell proliferation and epithelial differentiation during lung maturation. *Dev Biol* **354**:242–252.
Jorstad NL, Wilken MS, Grimes WN, Wohl SG, VandenBosch LS, Yoshimatsu T, Wong RO, Rieke F, Reh TA. 2017. Stimulation of functional neuronal regeneration from Müller glia in adult mice. *Nature* **548**:103–107.
Jorstad NL, Wilken MS, Todd L, Finkbeiner C, Nakamura P, Radulovich N, Hooper MJ, Chitsazan A, Wilkerson BA, Rieke F, Reh TA. 2020. STAT Signaling Modifies Ascl1 Chromatin Binding and Limits Neural Regeneration from Muller Glia in Adult Mouse Retina. *Cell Rep* **30**:2195–2208.e5.
Joung J, Ma S, Tay T, Geiger-Schuller KR, Kirchgatterer PC, Verdine VK, Guo B, Arias-Garcia MA, Allen WE, Singh A, Kuksenko O, Abudayyeh OO, Gootenberg JS, Fu Z, Macrae RK, Buenrostro JD, Regev A, Zhang F. 2024. A transcription factor atlas of directed differentiation. *Cell* **187**:3161.
Le N, Appel H, Pannullo N, Hoang T, Blackshaw S. 2022. Ectopic insert-dependent neuronal expression of GFAP promoter-driven AAV constructs in adult mouse retina. *Front Cell Dev Biol* **10**:914386.
Lengner CJ, Welstead GG, Jaenisch R. 2008. The pluripotency regulator Oct4: a role in somatic stem cells? *Cell Cycle* **7**:725–728.
Le N, Vu T-D, Palazzo I, Pulya R, Kim Y, Blackshaw S, Hoang T. 2024. Robust reprogramming of glia into neurons by inhibition of Notch signaling and nuclear factor I (NFI) factors in adult mammalian retina. *Sci Adv* **10**:eadn2091.
Loh Y-H, Wu Q, Chew J-L, Vega VB, Zhang W, Chen X, Bourque G, George J, Leong B, Liu J, Wong K-Y, Sung KW, Lee CWH, Zhao X-D, Chiu K-P, Lipovich L, Kuznetsov VA, Robson P, Stanton LW, Wei C-L, Ruan Y, Lim B, Ng H-H. 2006. The Oct4 and Nanog transcription network regulates pluripotency in mouse embryonic stem cells. *Nat Genet* **38**:431–440.
Lyu P, Hoang T, Santiago CP, Thomas ED, Timms AE, Appel H, Gimmen M, Le N, Jiang L, Kim DW, Chen S, Espinoza DF, Telger AE, Weir K, Clark BS, Cherry TJ,

Qian J, Blackshaw S. 2021. Gene regulatory networks controlling temporal patterning, neurogenesis, and cell-fate specification in mammalian retina. *Cell Rep* **37**:109994.
Mo A, Mukamel EA, Davis FP, Luo C, Henry GL, Picard S, Urich MA, Nery JR, Sejnowski TJ, Lister R, Eddy SR, Ecker JR, Nathans J. 2015. Epigenomic Signatures of Neuronal Diversity in the Mammalian Brain. *Neuron* **86**:1369–1384.
Morrison GM, Brickman JM. 2006. Conserved roles for Oct4 homologues in maintaining multipotency during early vertebrate development. *Development* **133**:2011–2022.
Nelson BR, Ueki Y, Reardon S, Karl MO, Georgi S, Hartman BH, Lamba DA, Reh TA. 2011. Genome-wide analysis of Müller glial differentiation reveals a requirement for Notch signaling in postmitotic cells to maintain the glial fate. *PLoS One* **6**:e22817.
Niu W, Zang T, Smith DK, Vue TY, Zou Y, Bachoo R, Johnson JE, Zhang C-L. 2015. SOX2 reprograms resident astrocytes into neural progenitors in the adult brain. *Stem Cell Reports* **4**:780–794.
Niu W, Zang T, Zou Y, Fang S, Smith DK, Bachoo R, Zhang C-L. 2013. In vivo reprogramming of astrocytes to neuroblasts in the adult brain. *Nat Cell Biol* **15**:1164–1175.
Ocampo A, Reddy P, Martinez-Redondo P, Platero-Luengo A, Hatanaka F, Hishida T, Li M, Lam D, Kurita M, Beyret E, Araoka T, Vazquez-Ferrer E, Donoso D, Roman JL, Xu J, Rodriguez Esteban C, Nuñez G, Nuñez Delicado E, Campistol JM, Guillen I, Guillen P, Izpisua Belmonte JC. 2016. In Vivo Amelioration of Age-Associated Hallmarks by Partial Reprogramming. *Cell* **167**:1719–1733.e12.
Ohnishi K, Semi K, Yamamoto T, Shimizu M, Tanaka A, Mitsunaga K, Okita K, Osafune K, Arioka Y, Maeda T, Soejima H, Moriwaki H, Yamanaka S, Woltjen K, Yamada Y. 2014. Premature termination of reprogramming in vivo leads to cancer development through altered epigenetic regulation. *Cell* **156**:663–677.
Păun O, Tan YX, Patel H, Strohbuecker S, Ghanate A, Cobolli-Gigli C, Llorian Sopena M, Gerontogianni L, Goldstone R, Ang S-L, Guillemot F, Dias C. 2023. Pioneer factor ASCL1 cooperates with the mSWI/SNF complex at distal regulatory elements to regulate human neural differentiation. *Genes Dev* **37**:218–242.
Pavlou M, Probst M, Filippova E, Kaplan L, Prieve AR, Rieke F, Reh TA. 2024. AAV-mediated expression of proneural factors stimulates neurogenesis from adult Müller glia in vivo. *bioRxiv*. doi:10.1101/2024.09.13.612930
Pollak J, Wilken MS, Ueki Y, Cox KE, Sullivan JM, Taylor RJ, Levine EM, Reh TA. 2013. ASCL1 reprograms mouse Muller glia into neurogenic retinal progenitors. *Development* **140**:2619–2631.
Reyes-Aguirre LI, Lamas M. 2016. Oct4 Methylation-Mediated Silencing As an Epigenetic Barrier Preventing Müller Glia Dedifferentiation in a Murine Model of Retinal Injury. *Front Neurosci* **10**:523.
Rizzino A. 2013. Concise review: The Sox2-Oct4 connection: critical players in a much larger interdependent network integrated at multiple levels. *Stem Cells* **31**:1033–1039.
Sharma P, Gupta S, Chaudhary M, Mitra S, Chawla B, Khursheed MA, Ramachandran R. 2019. Oct4 mediates Müller glia reprogramming and cell cycle exit during retina regeneration in zebrafish. *Life Sci Alliance* **2**. doi:10.26508/lsa.201900548
Sim S-E, Park S-W, Choi S-L, Yu N-K, Ko H-G, Jang D-J, Lee K, Kaang B-K. 2011.

Assessment of the effects of virus-mediated limited Oct4 overexpression on the structure of the hippocampus and behavior in mice. *BMB Rep* **44**:793–798.
Surzenko N, Crowl T, Bachleda A, Langer L, Pevny L. 2013. SOX2 maintains the quiescent progenitor cell state of postnatal retinal Muller glia. *Development* **140**:1445–1456.
Takahashi K, Yamanaka S. 2006. Induction of pluripotent stem cells from mouse embryonic and adult fibroblast cultures by defined factors. *Cell* **126**:663–676.
Takashima S, Hirose M, Ogonuki N, Ebisuya M, Inoue K, Kanatsu-Shinohara M, Tanaka T, Nishida E, Ogura A, Shinohara T. 2013. Regulation of pluripotency in male germline stem cells by Dmrt1. *Genes Dev* **27**:1949–1958.
Uhlen M, Oksvold P, Fagerberg L, Lundberg E, Jonasson K, Forsberg M, Zwahlen M, Kampf C, Wester K, Hober S, Wernerus H, Björling L, Ponten F. 2010. Towards a knowledge-based Human Protein Atlas. *Nat Biotechnol* **28**:1248–1250.
Wang C, Rabadan Ros R, Martinez-Redondo P, Ma Z, Shi L, Xue Y, Guillen-Guillen I, Huang L, Hishida T, Liao H-K, Nuñez Delicado E, Rodriguez Esteban C, Guillen-Garcia P, Reddy P, Izpisua Belmonte JC. 2021. In vivo partial reprogramming of myofibers promotes muscle regeneration by remodeling the stem cell niche. *Nat Commun* **12**:3094.
Wang L-L, Serrano C, Zhong X, Ma S, Zou Y, Zhang C-L. 2021. Revisiting astrocyte to neuron conversion with lineage tracing in vivo. *Cell* **184**:5465–5481.e16.
Wang S, Sengel C, Emerson MM, Cepko CL. 2014. A gene regulatory network controls the binary fate decision of rod and bipolar cells in the vertebrate retina. *Dev Cell* **30**:513–527.
Wan J, Goldman D. 2016. Retina regeneration in zebrafish. *Curr Opin Genet Dev* **40**:41–47.
Xiao D, Jin K, Qiu S, Lei Q, Huang W, Chen H, Su J, Xu Q, Xu Z, Gou B, Tie X, Liu F, Liu S, Liu Y, Xiang M. 2021. Regeneration of Ganglion Cells for Vision Restoration in Mammalian Retinas. *Front Cell Dev Biol* **9**:755544.
Xie Y, Zhou J, Chen B. 2022. Critical examination of Ptbp1-mediated glia-to-neuron conversion in the mouse retina. *Cell Rep* **39**:110960.
Yao K, Qiu S, Wang YV, Park SJH, Mohns EJ, Mehta B, Liu X, Chang B, Zenisek D, Crair MC, Demb JB, Chen B. 2018. Restoration of vision after de novo genesis of rod photoreceptors in mammalian retinas. *Nature* **560**:484–488.
Yu J-H, Nam B-G, Kim M-G, Pyo S, Seo J-H, Cho S-R. 2021. Expression of Reprogramming Factor OCT4 Ameliorates Myelination Deficits and Induces Striatal Neuroprotection in Huntington's Disease. *Genes* **12**. doi:10.3390/genes12050712
Zalc A, Sinha R, Gulati GS, Wesche DJ, Daszczuk P, Swigut T, Weissman IL, Wysocka J. 2021. Reactivation of the pluripotency program precedes formation of the cranial neural crest. *Science* **371**. doi:10.1126/science.abb4776

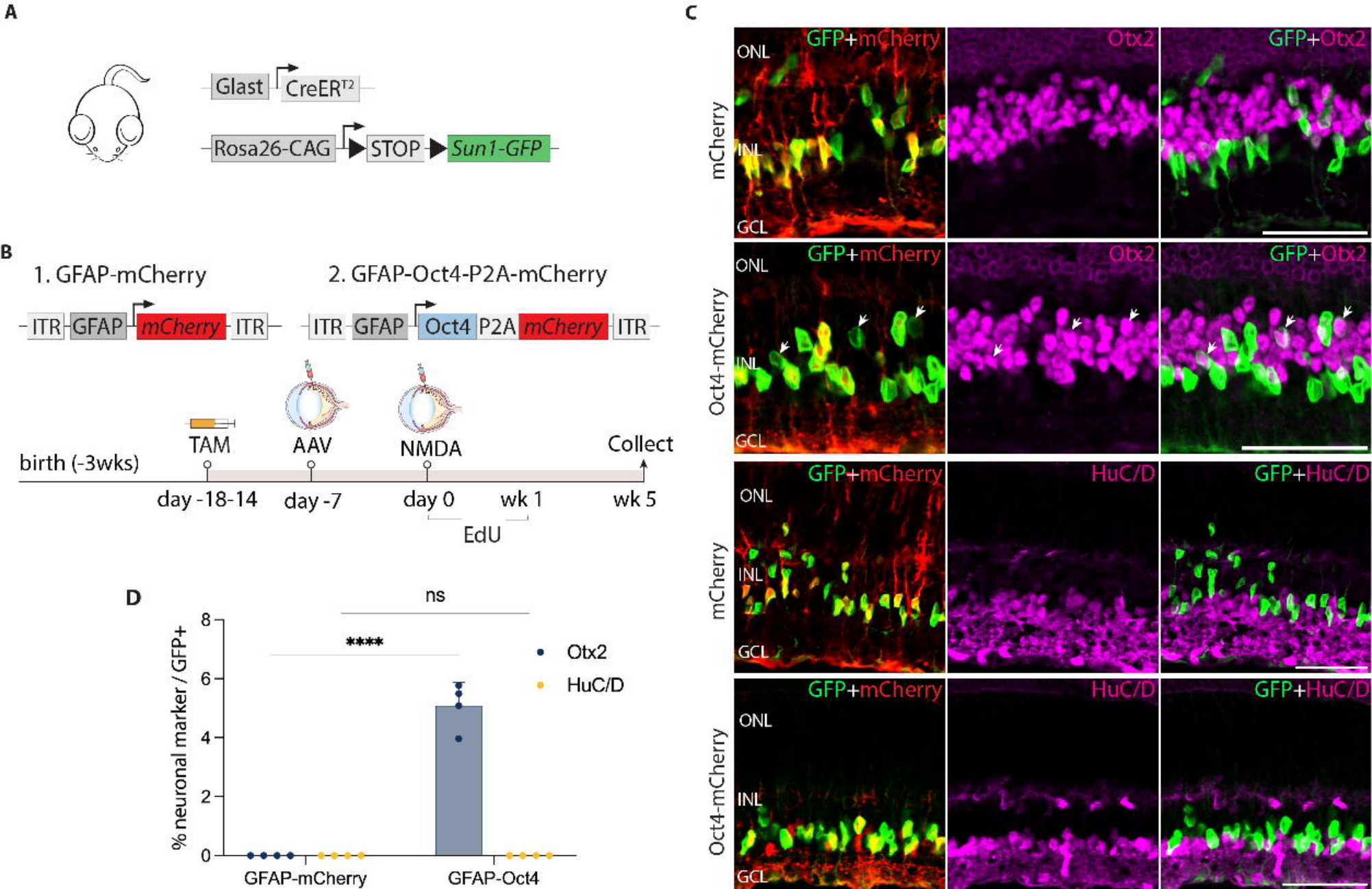
A
Glast
CreER^{T2}
Rosa26-CAG
STOP
Sun1-GFP
B
1. GFAP-mCherry
ITR
GFAP
mCherry
ITR
2. GFAP-Oct4-P2A-mCherry
ITR
GFAP
Oct4
P2A
mCherry
ITR
TAM
AAV
NMDA
Collect
birth (-3wks)
day -18-14
day -7
day 0
wk 1
wk 5
EdU
C
GFP+mCherry
Otx2
GFP+Otx2
HuC/D
GFP+HuC/D
ONL
INL
GCL
mCherry
Oct4-mCherry
D
ns
****
% neuronal marker / GFP+
0
2
4
6
8
Otx2
HuC/D
GFAP-mCherry
GFAP-Oct4

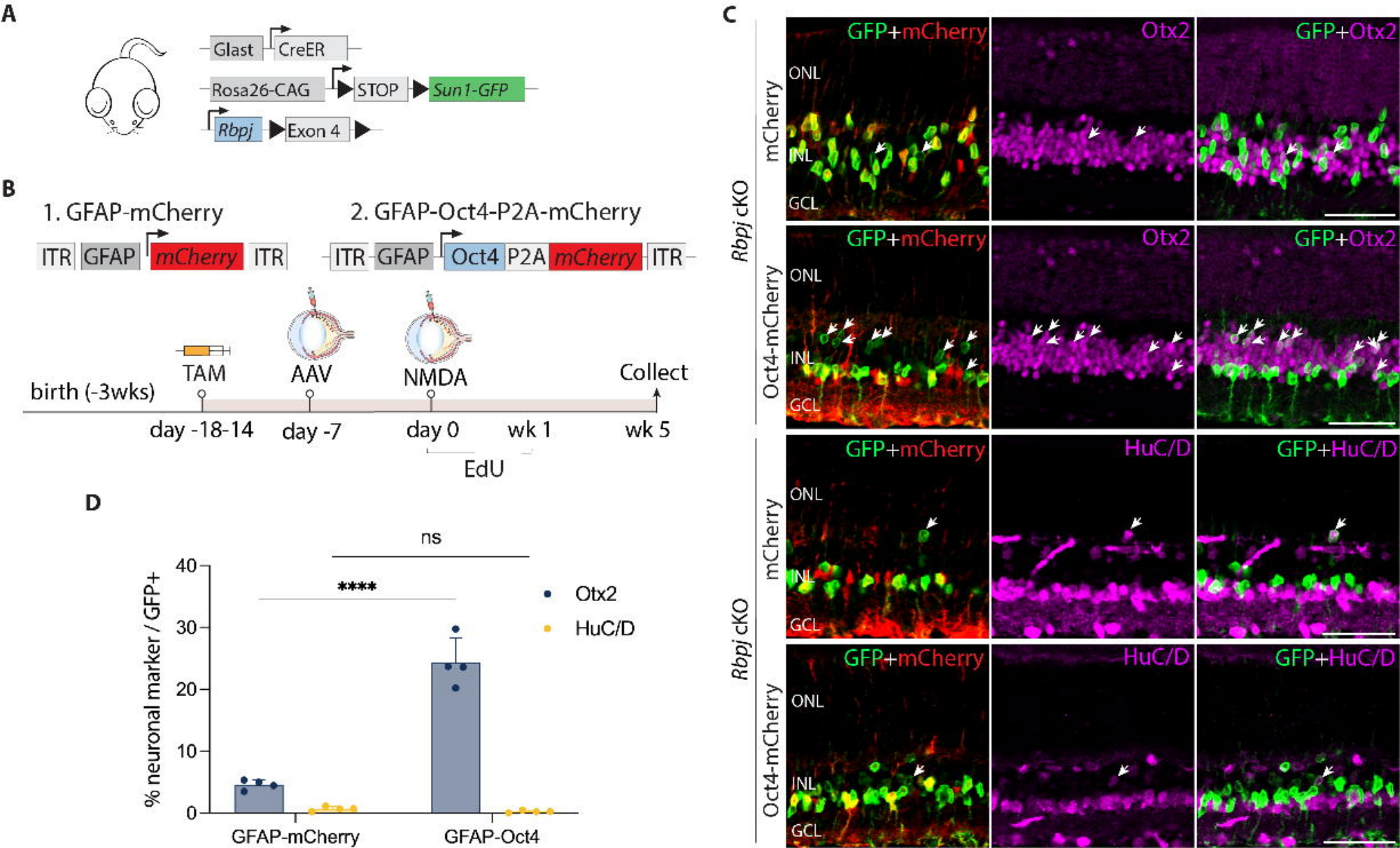
A
Glast
CreER
Rosa26-CAG
STOP
Sun1-GFP
Rbpj
Exon 4
B
1. GFAP-mCherry
ITR
GFAP
mCherry
ITR
2. GFAP-Oct4-P2A-mCherry
ITR
GFAP
Oct4
P2A
mCherry
ITR
TAM
AAV
NMDA
Collect
birth (-3wks)
day -18-14
day -7
day 0
wk 1
wk 5
EdU
C
Rbpj cKO
mCherry
Oct4-mCherry
GFP+mCherry
Otx2
GFP+Otx2
HuC/D
GFP+HuC/D
ONL
INL
GCL
D
% neuronal marker / GFP+
ns
****
Otx2
HuC/D
GFAP-mCherry
GFAP-Oct4

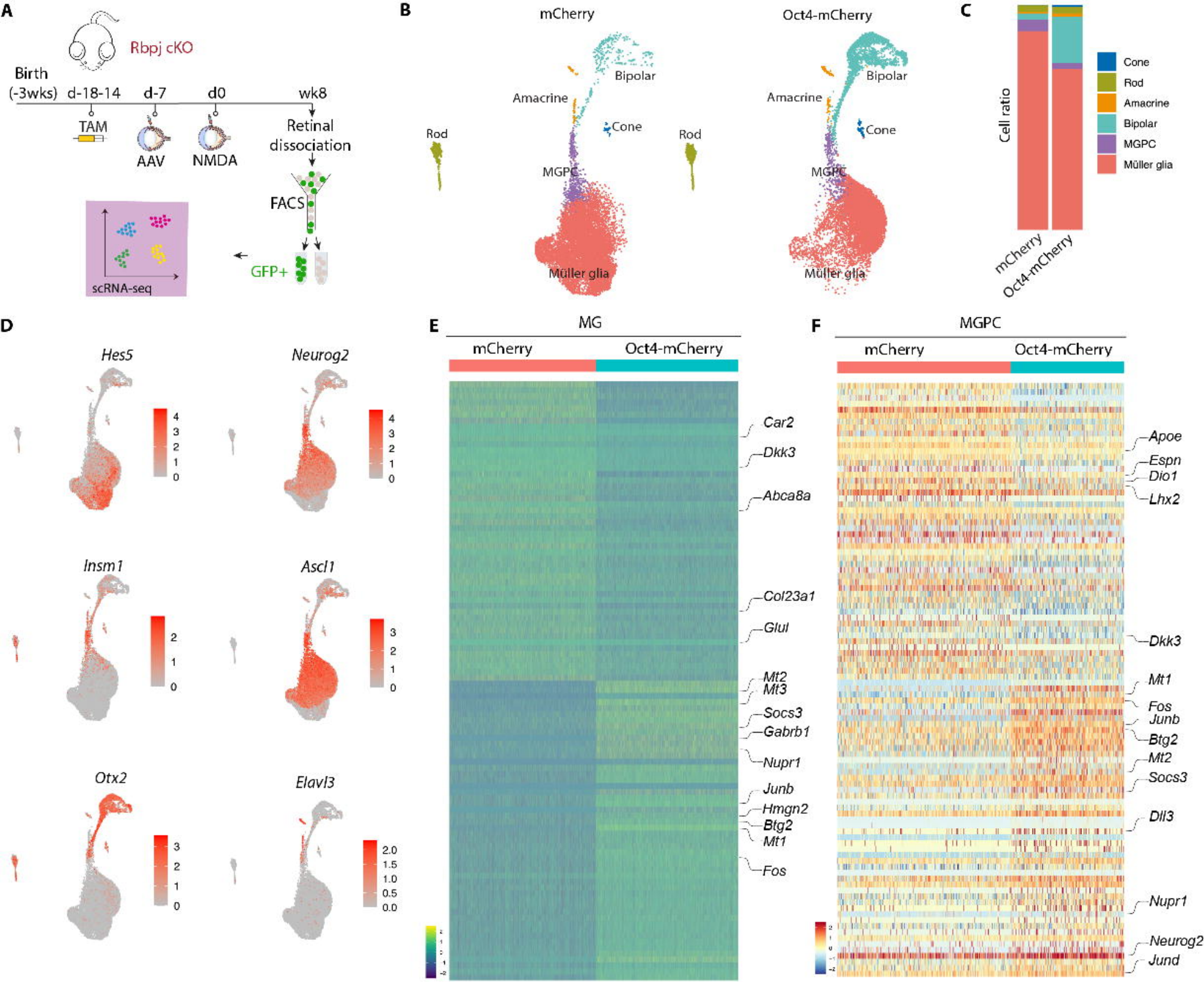
A
Rbpj cKO
Birth
(-3wks)
d-18-14
d-7
d0
wk8
TAM
AAV
NMDA
Retinal dissociation
FACS
GFP+
scRNA-seq
B
mCherry
Oct4-mCherry
Rod
Amacrine
Bipolar
Cone
MGPC
Müller glia
C
Cell ratio
mCherry
Oct4-mCherry
Cone
Rod
Amacrine
Bipolar
MGPC
Müller glia
D
Hes5
Neurog2
Insm1
Ascl1
Otx2
Elavl3
E
MG
mCherry
Oct4-mCherry
Car2
Dkk3
Abca8a
Col23a1
Glul
Mt2
Mt3
Socs3
Gabrb1
Nupr1
Junb
Hmgn2
Btg2
Mt1
Fos
F
MGPC
mCherry
Oct4-mCherry
Apoe
Espn
Dio1
Lhx2
Dkk3
Mt1
Fos
Junb
Btg2
Mt2
Socs3
Dll3
Nupr1
Neurog2
Jund

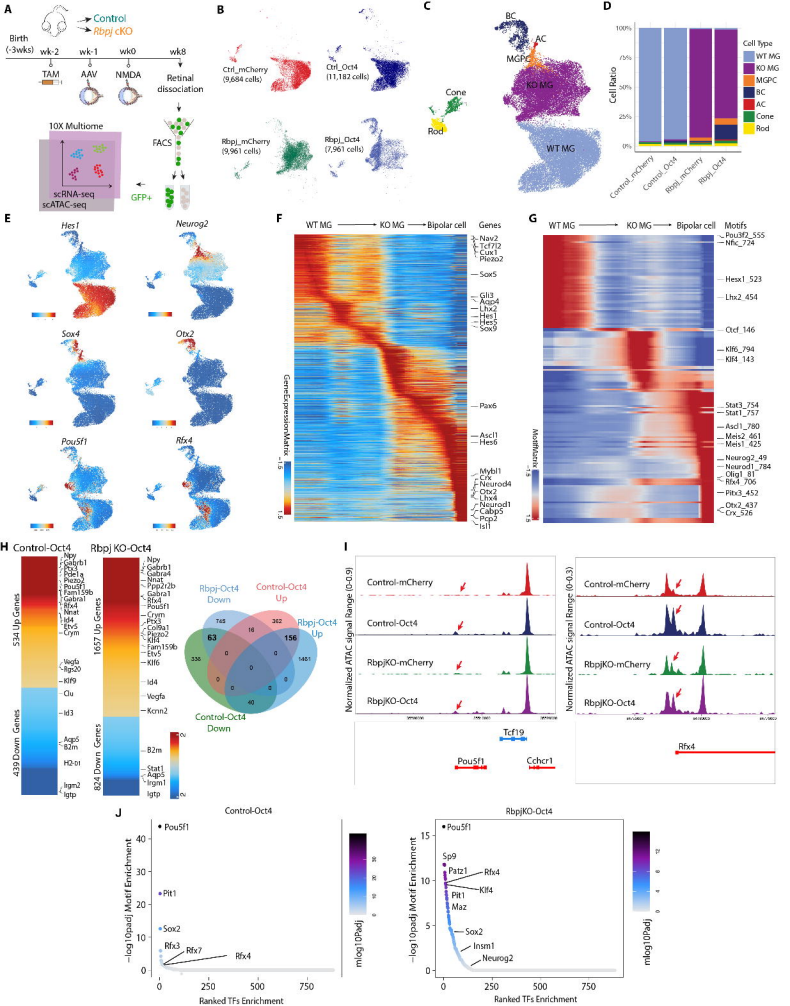
A
Control
Rbpj cKO
Birth (~3wks)
wk-2
wk-1
wk0
wk8
TAM
AAV
NMDA
Retinal dissociation
10X Multiome
FACS
scRNA-seq
scATAC-seq
GFP+
B
Ctrl_mCherry (9,684 cells)
Ctrl_Oct4 (11,182 cells)
Rbpj_mCherry (9,961 cells)
Rbpj_Oct4 (7,961 cells)
C
BC
AC
MGPC
KO MG
Cone
Rod
WT MG
D
Cell Ratio
Cell Type
WT MG
KO MG
MGPC
BC
AC
Cone
Rod
Control_mCherry
Control_Oct4
Rbpj_mCherry
Rbpj_Oct4
E
Hes1
Neurog2
Sox4
Otx2
Pou5f1
Rfx4
F
WT MG → KO MG → Bipolar cell
Genes
GeneExpressionMatrix
Nxv2
Tcf712
Cux1
Plxna2
Sox5
Gli3
Aqp4
Lhx2
Hes1
Hes5
Sox9
Pax6
Ascl1
Hes6
Mybl1
Crx
Neurod4
Otx2
Lhx4
Neurod1
Cabp5
Pcp2
Isl1
G
WT MG → KO MG → Bipolar cell
Motifs
MotifMatrix
Pou3f2_555
Nfic_724
Hesx1_523
Lhx2_454
Ctcf_146
Klf6_794
Klf4_143
Stat3_754
Stat1_757
Ascl1_780
Meis2_461
Meis1_425
Neurog2_49
Neurod1_784
Olig1_81
Rfx4_706
Pitx3_452
Otx2_437
Crx_526
H
Control-Oct4
Rbpj KO-Oct4
534 Up Genes
439 Down Genes
1637 Up Genes
824 Down Genes
Npy
Gabrb1
Pitx3
Plxna2
Pitx1
Pou5f1
Fam159b
Gabra1
Rfx4
Neat
Id4
Etv5
Crym
Vegfa
Rgs20
Klf9
Clu
Id3
Acp5
B2m
H2-D1
Irgm2
Igtp
Cpne4
Gabra4
Ppp2r2b
Gabra1
Rfx4
Pou5f1
Crym
Pitx3
Cobra1
Plxna2
Klf4
Fam159b
Etv5
Klf6
Id4
Vegfa
Kcnn2
B2m
Stat1
Aqp5
Irgm1
Igtp
Rbpj-Oct4 Down
Control-Oct4 Up
Rbpj-Oct4 Up
Control-Oct4 Down
745
16
382
63
156
336
1461
40
I
Normalized ATAC signal Range (0-0.9)
Control-mCherry
Control-Oct4
RbpjKO-mCherry
RbpjKO-Oct4
Tcf19
Pou5f1
Cchcr1
Rfx4
J
Control-Oct4
RbpjKO-Oct4
−log10padj Motif Enrichment
Ranked TFs Enrichment
mlog10Padj
Pou5f1
Pit1
Sox2
Rfx3
Rfx7
Rfx4
Sp9
Patz1
Klf4
Maz
Insm1
Neurog2